Polymer 300 (2024) 126988

Contents lists available at ScienceDirect

Polymer

journal homepage: www.elsevier.com/locate/polymer

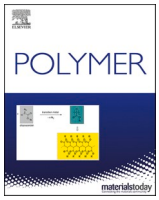

Bifunctional luminescent conjugated microporous polymers containing BODIPY and tetraphenylethene units for highly efficient energy storage and enhanced sensing of Cu^{2+} ions

Awad I. Said [a,b,1], Mohamed Gamal Mohamed [a,c,**,1], Manivannan Madhu [d,1], Poonam Nagendr Singh [c], Swetha V Chaganti [d], Mohamed Hammad Elsayed [e], Wei Lung Tseng [d,f,g], Françisco M. Raymo [b], Shiao-Wei Kuo [c,h,*]

[a] Chemistry Department, Faculty of Science, Assiut University, Assiut, 71515, Egypt
[b] Laboratory for Molecular Photonics, Department of Chemistry, University of Miami, 1301 Memorial Drive, Coral Gables, FL, 33146-0431, USA
[c] Department of Materials and Optoelectronic Science, Center of Crystal Research, National Sun Yat-Sen University, Kaohsiung, 804, Taiwan
[d] Department of Chemistry, National Sun Yat-sen University, Kaohsiung, 804, Taiwan
[e] Department of Chemistry, Faculty of Science, Al-Azhar University, Nasr City, Cairo, 11884, Egypt
[f] Department of Chemistry and Center for Nanoscience and Nanotechnology, National Sun Yat-sen University, Kaohsiung, 80424, Taiwan
[g] School of Pharmacy, College of Pharmacy, Kaohsiung Medical University, Kaohsiung, 80708, Taiwan
[h] Department of Medicinal and Applied Chemistry, Kaohsiung Medical University, Kaohsiung, 807, Taiwan

ARTICLE INFO

Keywords:
Borondipyrromethene
Tetraphenylethene
Conjugated microporous polymers

ABSTRACT

Here, using the Sonogashira coupling technique, a new fluorescent tetraphenylethene (TPE) and borondipyrromethene (BODIPY)-based CMP (TPE-BODIPY-CMP) was built and developed for usage in supercapacitors and Cu^{2+} ion detection. XPS, ssNMR, and FTIR techniques were used to validate the presence of the functional groups, aromatic carbons, and atoms [Si, B, C, N, O, and F] in the TPE-BODIPY-CMP framework. In the TPE-BODIPY-CMP, the calculated pore size, S_{BET}, and carbon residue were 1.52–2.82 nm, 300 $m^2\ g^{-1}$, and 67%, respectively. as per our electrochemical test, the capacitance stability [83.23% after 5000 cycles], and specific capacity of 176 F g^{-1} (0.5 A g^{-1}) for TPE-BODIPY-CMP. We performed photoluminescence (PL) experiments on TPE-BODIPY-CMP to evaluate its capacity in cation detection [Cu^{2+}, Pb^{2+}, Al^{3+}, Cr^{3+}, Ni^{2+}, Ce^{3+}, Mg^{2+}, Hg^{2+}, Fe^{3+}, Fe^{2+}, Zn^{2+}, and Ag^{+}] and a limit of detection (LOD) of TPE-BODIPY-CMP toward Cu^{2+} ions was 2.5×10^{-7} M.

1. Introduction

Due to their unique properties such as low maintenance costs, high power density, extended cycle stability, and quick charge/discharge rates, supercapacitors (SCs) are gaining a lot of interest as environmentally friendly energy storage devices [1–16]. Electrical double-layer capacitors (EDLCs) and pseudo-capacitors with immediately reversible redox processes are the two primary kinds of SCs [17–20]. Activated carbon (ACs) is known for its high surface area, porous structure, outstanding conductivity, and remarkable electrochemical stability. These attributes are frequently the foundation of the latter. An electrical double layer is created to store electrical energy [21]. Pseudocapacitors have benefits, however they are limited by things like capacitance and relatively poor energy density.

One potential solution to these constraints is the creation of materials with large surface areas and hierarchical porous structures [22]. In such structures, micropores enhance the capacitance of EDLCs, mesopores create low-resistance paths for ion migration within porous materials, and macropores act as ion buffering reservoirs, reducing ion diffusion distances. In addition to porous architectures, heteroatom doping, involving elements like nitrogen [23], sulfur [24], boron [25], fluorine [26], and others, emerges as an effective technique for enhancing

* Corresponding author. Department of Materials and Optoelectronic Science, Center of Crystal Research, National Sun Yat-Sen University, Kaohsiung, 804, Taiwan.
** Corresponding author. Chemistry Department, Faculty of Science, Assiut University, Assiut, 71515, Egypt.
E-mail addresses: mgamal.eldin12@yahoo.com (M. Gamal Mohamed), kuosw@faculty.nsysu.edu.tw (S.-W. Kuo).
[1] These authors contributed equally.

https://doi.org/10.1016/j.polymer.2024.126988
Received 4 January 2024; Received in revised form 20 March 2024; Accepted 27 March 2024
Available online 31 March 2024

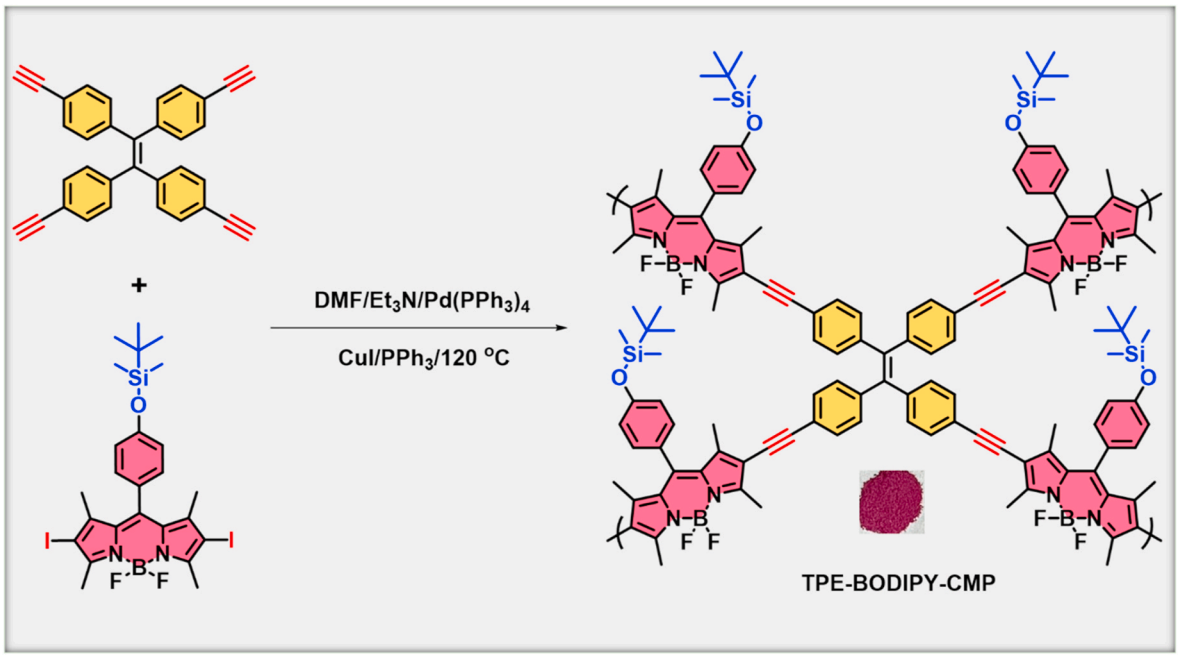

Fig. 1. The synthetic approach of TPE-BODIPY-CMP through the Sonogashira reaction.

material properties, spanning gas separation and electrical performance [27]. The introduction of boron, with its lower electronegativity and one fewer electron in the valence layer compared to carbon, influences the oxidation and conductive characteristics of materials. Nitrogen doping contributes to improved electrical performance through the pseudocapacitance effect of nitrogen atoms [28]. Meanwhile, the exceptionally high electronegativity of fluorine makes it valuable in energy conversion and storage systems, enhancing rate capability, cycle stability, and wettability [29]. Furthermore, co-doping, involving the introduction of multiple heteroatoms, proves advantageous over solitary heteroatom doping by exerting a synergistic impact, enhancing the overall performance of electrode materials [30,31].

Over an extensive period, CMPs are the focus of much investigation. A wide range of applications are made possible by their chemical stability, significant S_{BET}, varied pore sizes, improved electrical conductivity, and reduced density in comparison to inorganic materials [32–35]. These include pollutant removal, H_2 evolution, sensing of metal ions, energy storage, and utilization as positive electrode materials in lithium-sulfur batteries. The pi-conjugated structure of CMPs, coupled with their redox activity, imparts outstanding electrochemical performance and luminous properties [36–40]. Furthermore, various techniques, such as Yamamoto coupling, Sonogashira-Hagihara, and oxidative polymerization, can be employed for the production of CMPs, leading to diverse structures and characteristics in the resulting materials [40–45].

Among the huge number of known fluorescent dyes, borondipyrromethene (hereafter known as BODIPY) chromophores have attracted the attention of chemists, physicists, and biochemists after their discovery by Treibs and co-workers [46]. The extensive π-system they possess exhibits high molar absorption coefficients (>70 m M^{-1} cm^{-1}) and absorbs light in the green segment of the visible spectrum. The bathochromically shifted S0→S1 absorption can be moved up to the far-red or near-infrared region by a suitable substitute offering further electronic delocalization. After being excited, BODIPYs release light with high luminescence quantum yields and modest Stokes shifts (10 and 20 nm). If substituents lack heavy atoms that induce intersystem crossing and do not contain groups that might initiate photoinduced electron transfer, the latter parameter can approach unity. BODIPY dyes demonstrate relative stability when potent acids or nucleophiles are avoided [47–49]. A variety of applications for BODIPY dyes have been reported including biomolecular labeling [50], chromogenic cation probes [51,52], photodynamic therapy [53], fluorescent switches [54], electroluminescent materials [55], laser dyes [56], light-harvesters [57] and photosensitizers for solar cells [58]. Conversely, due to their good photophysical characteristics and possible uses in functional materials, BODIPY-related compounds are trendy study subjects [59,60]. POPs were prepared with BODIPY units in a limited number of studies, and their use was exclusive to heterogeneous photocatalysis, CO_2 uptake, water treatment, and I_2 adsorption [61-65].

TPE stands out as a promising ingredient for creating vibrant materials due to its uncomplicated and uniform chemical composition [61–63]. Employing the McMurry coupling technique allows for the straightforward production of both pristine TPE and its various topological variations. As a representative AIE luminophore, TPE possesses a propeller-like structure and a straightforward molecular arrangement, establishing it as an archetype for luminogens. While the solution state fluorescence emission of TPE and its derivatives appear subdued, aggregation state conditions lead to heightened fluorescence emission [64–66]. Copper (Cu^{2+}) cations play a vital role in many of the biological processes. It's important for electron transfer in cellular respiration, and functions as redox regulators [67]. However, its abnormal level is responsible for various diseases including Wilson [68] and Alzheimer's [69]. According to the U.S. Environmental Protection Agency (EPA), the maximum acceptable concentration of Cu^{2+} in water for drinking is 20 μM [70]. Recently, analytical techniques based on fluorescence emission attracted scientists' attention for detecting different analysts due to their advantages such as high sensitivity, no reference requirement, rapid detection, and bioimaging capability [71–76]. Until now, there hasn't been any documented information on the synthesis of POP, incorporating TEP and BODIPY functionalities as building monomers. This polymer has the potential for utilization as an electrode material in energy storage and for chemical sensing applications, particularly in detecting Cu^{2+}.

Utilizing the Sonogashira coupling process in conjunction with the previously provided information, we successfully synthesized the distinctive TPE-BODIPY-CMP as a purple solid, incorporating both TPE and BODIPY units. This synthesis involved the reaction of TPE-T with BODIPY-I_2 in a DMF/Et_3N solution, utilizing $Pd(PPh_3)_4$ as a catalyst

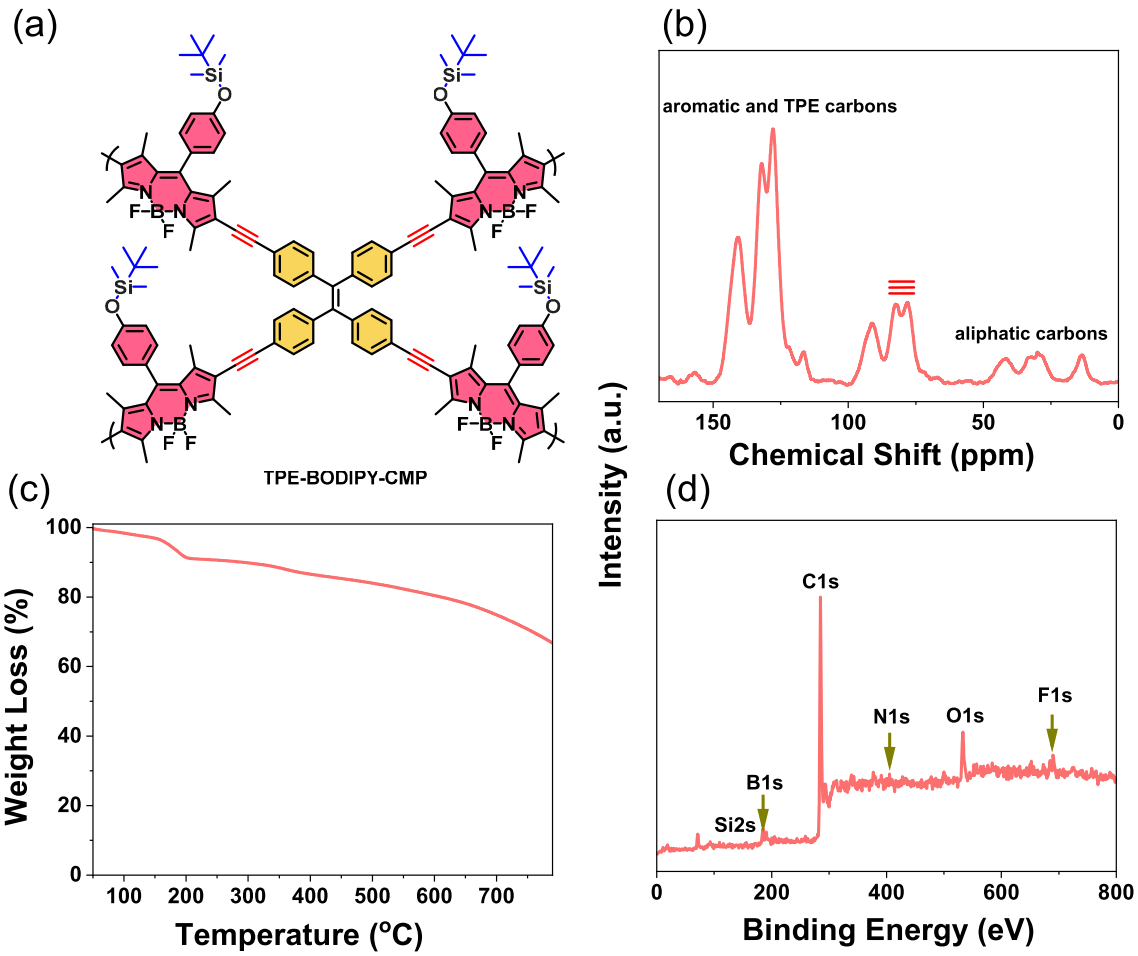

Fig. 2. (a) The molecular chemical structure, (b) FTIR, (c) TGA, and (d) XPS profiles of TPE-BODIPY-CMP.

[Fig. 1]. The framework structure of TPE-BODIPY-CMP was scrutinized through XPS, ssNMR, and FTIR. Additionally, the thermal behavior of the TPE-BODIPY-CMP architecture was assessed using TGA. Furthermore, TPE-BODIPY-CMP exhibited a S_{BET} of 300 $m^2\ g^{-1}$ and a pore size of ca 1.52–2.82 nm. Based on our testing results, TPE-BODIPY-CMP showed an excellent capacitive of 176 F g^{-1} at 0.5 A g^{-1} concerning electrochemical performance. It is noteworthy that even after 5000 cycles, this TPE-BODIPY-CMP retains an astounding 83.23% of its capacitance. The detection of the TPE-BODIPY-CMP framework toward different cations [Cu^{2+}, Pb^{2+}, Al^{3+}, Cr^{3+}, Ni^{2+}, Ce^{3+}, Mg^{2+}, Hg^{2+}, Fe^{3+}, Fe^{2+}, Zn^{2+}, and Ag^{+}] was carefully examined through PL tests. Its extraordinary sensitivity to Cu^{2+} ions was highlighted by the findings, which showed a LOD of 2.5×10^{-7} M. In summary, the TPE-BODIPY-CMP material exhibits exceptional thermal properties, porosity, and electrochemical characteristics, rendering it a highly attractive option for various applications, such as the detection of Cu^{2+} ions and supercapacitors.

2. Experimental section

2.1. Materials

The specified materials were sourced from Sigma-Aldrich and Across, including Zn, 2,3-dichloro-5,6-dicyano-1,4-benzoquinone (DDQ, 98%), trifluoroacetic acid (TFA, 99%), *tert*-butyldimethylsilyl chloride (*tert*-$BDSiCl_2$, 98%), triethylamine (Et_3N, 99.5%), 4-hydroxybenzalehyde (98%), benzophenone (99%), titanium tetrachloride ($TiCl_4$, 99.9%), methanol (MeOH), N-iodosuccinimide (95%), tetrahydrofuran (THF), 2,4-dimethylpyrrole (DMPy, 97%), N,N-dimethylformamide (DMF), boron trifluoride diethyl etherate (BF_3OEt_2), triphenylphosphine (PPh_3, 99%), tetrakis(triphenylphosphine)palladium(0) ($Pd(PPh_3)_4$), copper(I) iodide (CuI, 99.5%), and dichloromethane (CH_2Cl_2). Synthesis of TPE-TMS and TPE-T was performed according to known protocols described in the literature and their spectroscopic data [including NMR and FTIR,Scheme S1 and Figs. S1–S6] [77–79].

2.2. Synthesis of 4-(tert-butyldimethylsilyloxy)benzaldehyde [tert-BDMSi-BZ]

Dissolving *tert*-$BDSiCl_2$ (3.92 g, 24.4 mmol), Et_3N (3.6 ml, 24.4 mmol), 4-hydroxybenzaldehyde (2 g, 16.4 mmol) in CH_2Cl_2 (80 mL) and the reaction solution was kept and stirred for 10 h. The resulting solution was extracted with H_2O and CH_2Cl_2. After the workup process, the product was subjected to purification using a column chromatography method (hexane/EtOAc = 10/1), resulting in the *tert*-BDMSi-BZ as a yellow oil (3.48 g, 90%,Scheme S2). ^{1}H NMR (Fig. S7): δ 9.79 (s, 1H), 7.69 (d, 2H), 6.85 (d, 2H), 0.89 (s, 9H), 0.15 (s, 6H).

2.3. Synthesis of meso-(tert-butyldimethyl(phenoxy)silane) appended BODIPY [tert-BDMSi-BODIPY]

In the presence of an argon atmosphere, *tert*-BDMSi-BZ (2.0 mmol, 0.47 g) and DMPy (4.5 mmol, 0.43 g) in dry CH_2Cl_2 (25 mL). Two drops of TFA were added to the reaction mixture [kept stirring for 12 h at 25 °C]. Following this, a solution of DDQ (2.0 mmol, 0.45 g) in 10 mL CH_2Cl_2 was added dropwise for 30 min. Subsequently, 6 mL of BF_3OEt_2 and 6 mL of Et_3N were sequentially introduced and kept the reaction for

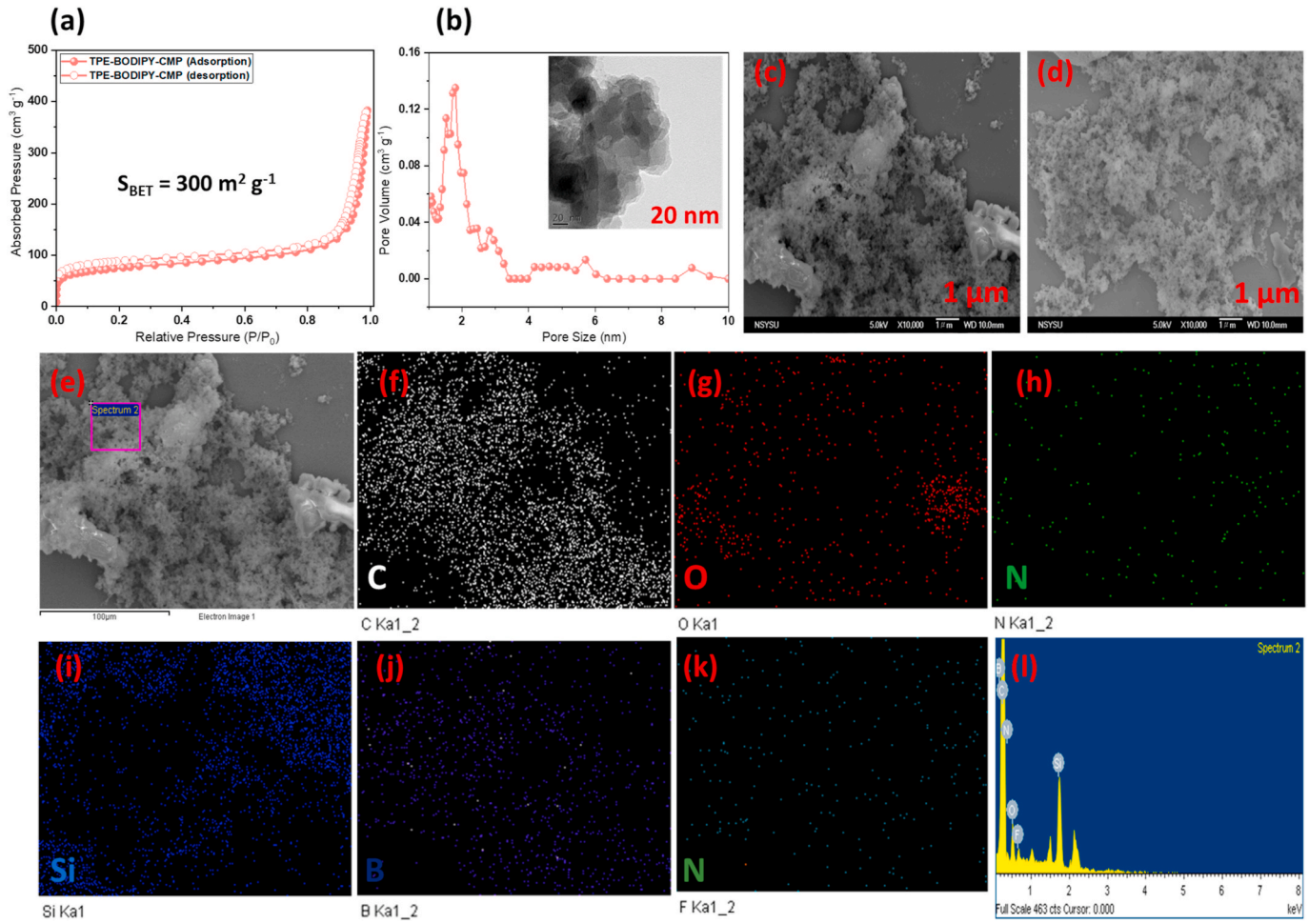

Fig. 3. (a) BET, (b) pore size, (c, d) SEM, (e–l) SEM-EDS mapping profiles [for Si, B, C, N, O, F atoms] of TPE-BODIPY-CMP. [photo inset Fig. 3(b) for TEM image of the TPE-BODIPY-CMP].

10 h. After purifying the crude product using column chromatography (EtOAc: hexane = 1:10), a red solid product was produced [Scheme S3]. Yield: 0.7 g (35%). ^{1}H NMR (300 MHz, Fig. S8) δ 6.83 (dd, J = 47.6, 8.4 Hz, 4H), 5.75 (s, 2H), 2.33 (s, 6H), 1.22 (s, 6H), 0.79 (s, 9H). ^{13}C NMR (126 MHz, Fig. S9) δ 156.47, 155.26, 143.13, 141.93, 131.77, 129.20, 127.96, 121.10, 25.68, 18.34, 14.56, 14.40, −4.40. ESI-TOF mass spectrum 455.25 (57 %, M^++1, Fig. S10).

2.4. Synthesis of 2,6-diiodo-substituted meso-(tert-butyldimethyl (phenoxy)silane) appended BODIPY [BODIPY-I_2]

With stirring, *tert*-BDMSi-BODIPY (0.2 g, 0.44 mmol) and N-iodosuccinimide (0.48 g, 2.1 mmol) were mixed with dry DCM (30 mL) in the dark at RT for 12 h in room temperature. The red solution was washed using H_2O (100 mL × 2). The BODIPY-I_2 was purified using a similar method to the *tert*-BDMSi-BODIPY to give a red solid (0.11 g, 66%, Scheme S4). FTIR (Fig. S11): 3031.78, 2925.58, 2843.41 cm^{-1}. ^{1}H NMR (Fig. S12) δ 7.07 (dd, J = 48.4, 8.0 Hz, 4H), 2.66 (s, 6H), 1.48 (s, 6H), 1.04 (s, 9H). ^{13}C NMR (Fig. S13) δ 155.94, 155.56, 144.30, 140.62, 130.62, 128.07, 126.59, 120.42, 84.53, 24.65, 17.35, 16.00, 14.98, −5.45. ESI-TOF mass spectrum 678.04 (100%, M^+, Fig. S14).

2.5. Synthesis of TPE- BODIPY-CMP

In a Pyrex tube, DMF (10 mL) and Et_3N (10 mL) were introduced to a mixture containing TPE-T (0.3 g, 0.7 mmol), BODIPY-I_2 (0.99, 1.4 mmol), CuI (3 mg), PPh_3 (5 mg), and $Pd(PPh_3)_4$ (1.5 mg, 0.013 mmol). Following three cycles of freeze, pump, and thaw, the resulting liquid was homogenized and then heated to 110 °C for three days. The mixture underwent filtration and subsequent washing with MeOH, and acetone as part of the Sonogashira coupling process to form TPE- BODIPY-CMP as a violet powder with a yield of 75%.

3. Results and discussion

3.1. Synthesis and characterization of BODIPY-I_2 and TPE-BODIPY-CMP framework

Schemes S2-S4 carried out the synthesis of the monomer BODIPY-I_2. Initially, the phenolic OH group of 4-hydroxybenzaldehyde was protected by tert-butyldimethylsilyl chloride, yielding *tert*-BDMSi-BZ. Subsequently, tert-BDMSi-BZ underwent a reaction with 2,4-dimethylpyrrole in dried DCM under argon protection, followed by oxidation using DDQ and reaction with BF_3OEt_2 to produce *tert*-BDMSi-BODIPY. The final BODIPY-I_2 was obtained by reacting *tert*-BDMSi-BODIPY with *N*-iodosuccinimide in the absence of light. The synthetic substances' molecular structures were validated through ^{1}H NMR, ^{13}C NMR, and HR-mass spectra. The ^{1}H NMR spectrum of *tert*-BDMSi-BZ exhibited signals characteristic of aromatic protons (4H), aliphatic *tert*-butyl protons (9H), and highly shielded protons (6H) attached to silicon atoms. The ^{1}H NMR spectrum of tert-BDMSi-BODIPY revealed signals characteristic of meso substituent and pyrrole moiety protons (2H), with the pyrrole protons (2H) disappearing in the ^{1}H NMR spectrum of BODIPY-I_2, confirming the diiodonation of BODIPY. Furthermore, the

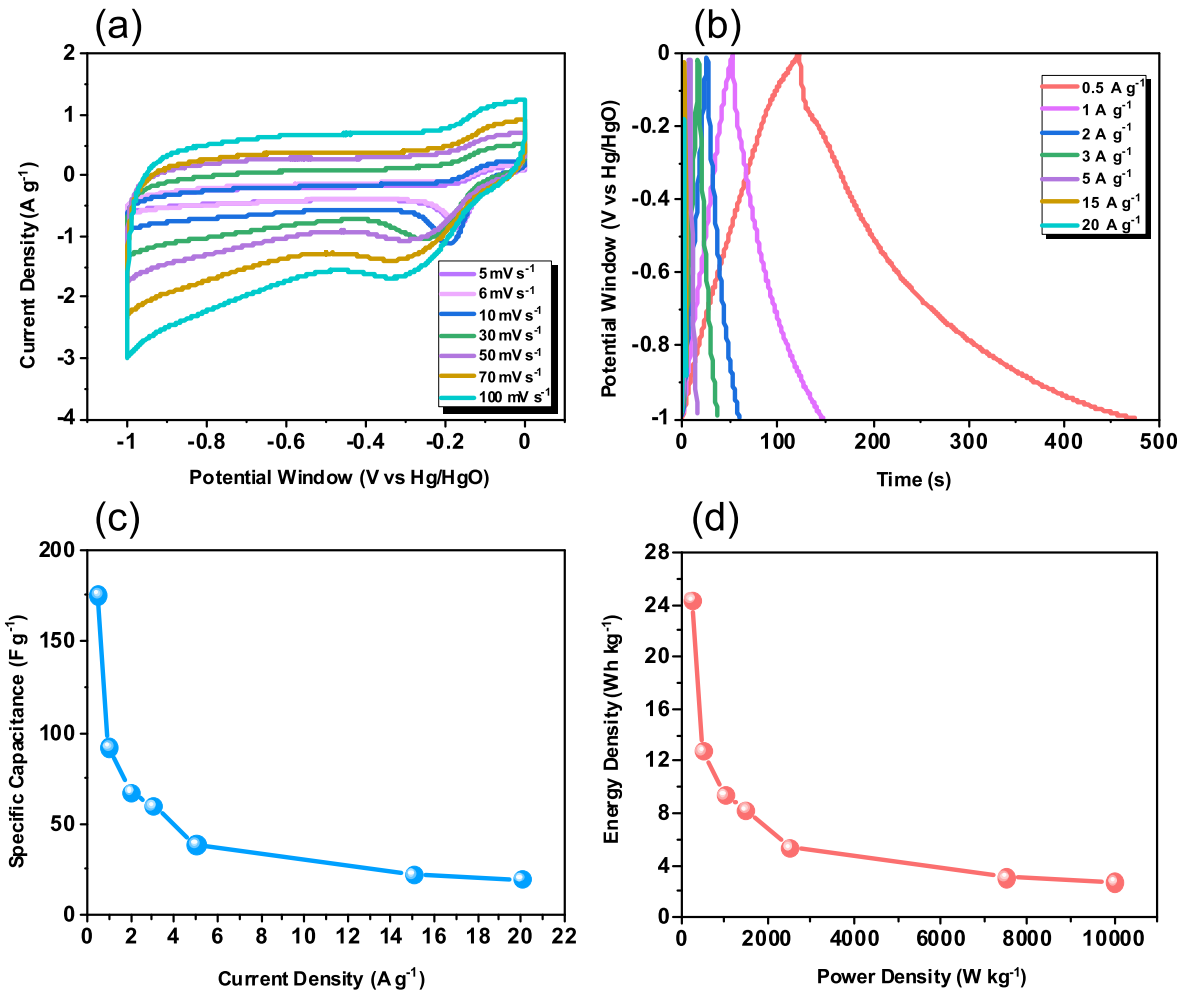

Fig. 4. (a) CV, (b) GCD, (c) specific capacitance, and (d) Ragone plot of TPE-BODIPY-CMP.

chemical structures of *tert*-BDMSi-BODIPY and BODIPY-I_2 were validated by their emission spectra. *tert*-BDMSi-BODIPY exhibited a strong emission at 515 nm upon excitation at 480 nm, whereas BODIPY-I_2 showed fluorescence quenching (Fig. S15) due to spin-orbital coupling of iodine atoms. The TPE-BODIPY-CMP framework was synthesized through the Sonogashira coupling method, which involved combining TPE-T and BODIPY-I_2 in a mixture of DMF and Et_3N (1:1 by volume). The resulting mixture was subjected to heating at 120 °C for 72 h. Subsequently, the obtained TPE-BODIPY-CMP framework was isolated as a purple powder, exhibiting insolubility in various solvents such as acetone, THF, DMF, MeOH, DCM, and EtOH, as illustrated in Fig. 1.

The chemical structure of the TPE-BODIPY-CMP framework (depicted in Fig. 2(a)) reveals characteristic signals in the aromatic carbon region for both BODIPY and TPE units (in the range of 157.18–116.68 ppm) [Fig. 2(b)]. Additionally, the signals corresponding to internal and terminal alkyne units are observed at 81.86 and 77.63 ppm, respectively. The ^{13}C CP/MAS spectrum [Fig. 2(b)] displays aliphatic groups within the BODIPY moiety, ranging from 40.93 to 13.59 ppm. Further confirmation of the aromatic CH, aliphatic CH, and alkyne units is evident in the TPE-BODIPY-CMP as displayed in FT-IR spectra (Fig. S16), where absorption bands at 3023, 2933, 2854, and 2024 cm^{-1}, respectively, support their presence. Furthermore, the thermal stability of the TPE-BODIPY-CMP framework was evidenced by its resistance to decomposition up to 291 °C. The carbon residue obtained from the TGA profile approached approximately 67 wt%, as illustrated in Fig. 2(c). Finally, the analysis of XPS data [Fig. 2(d)] confirmed the presence of Si, B, C, N, O, and F elements in the TPE-BODIPY-CMP sample. The peaks corresponding to these elements appeared at 154.95, 186.22, 285.73, 403.02, 533.8, and 686.62 eV, respectively, indicating the presence of Si, B, C, N, O, and F atoms in the framework.

Moreover, to assess the porosity of TPE-BODIPY-CMP, nitrogen adsorption tests were conducted at 77 K. The characteristic microporosity of TPE-BODIPY-CMP was evident from the reversible type-I isotherm, displaying a pronounced uptake within the low-pressure range. For TPE-BODIPY-CMP, the total pore volumes at $P/P_0 = 0.99$ were measured at 0.6 $cm^3\ g^{-1}$, and the Brunauer-Emmett-Teller (BET) surface area was determined to be 300 $m^2\ g^{-1}$ (refer to Fig. 3(a)). The pore size distribution curve for TPE-BODIPY-CMP, illustrated in Fig. 3 (b), indicates pore diameters (PD) of 1.52, 1.78, and 2.82 nm. The TEM image visually confirms the porous structure of TPE-BODIPY-CMP [inset Fig. 3(b)]. Furthermore, scanning electron microscopy (SEM) data [Fig. 3(c) and (d)] reveal a homogeneous granular-shaped aggregation morphology for TPE-BODIPY-CMP. The SEM-EDS mapping of the TPE-BODIPY-CMP sample revealed the presence of all elements—Si, B, C, N, O, and F—with respective atomic percentages of 3.39, 23.75, 68.68, 1.6, 2, and 0.58%. This distribution is illustrated in Fig. 3(e-l).

3.2. *Electrochemical performance of TPE-BODIPY-CMP framework*

The electrochemical performance of the TPE-BODIPY-CMP material was assessed using a three-electrode system, considering its boron, nitrogen, trace fluorine, and silicon content, as well as its attractive morphological properties and rational pore size distribution architecture. Cyclic voltammetry (CV) experiments were conducted on the

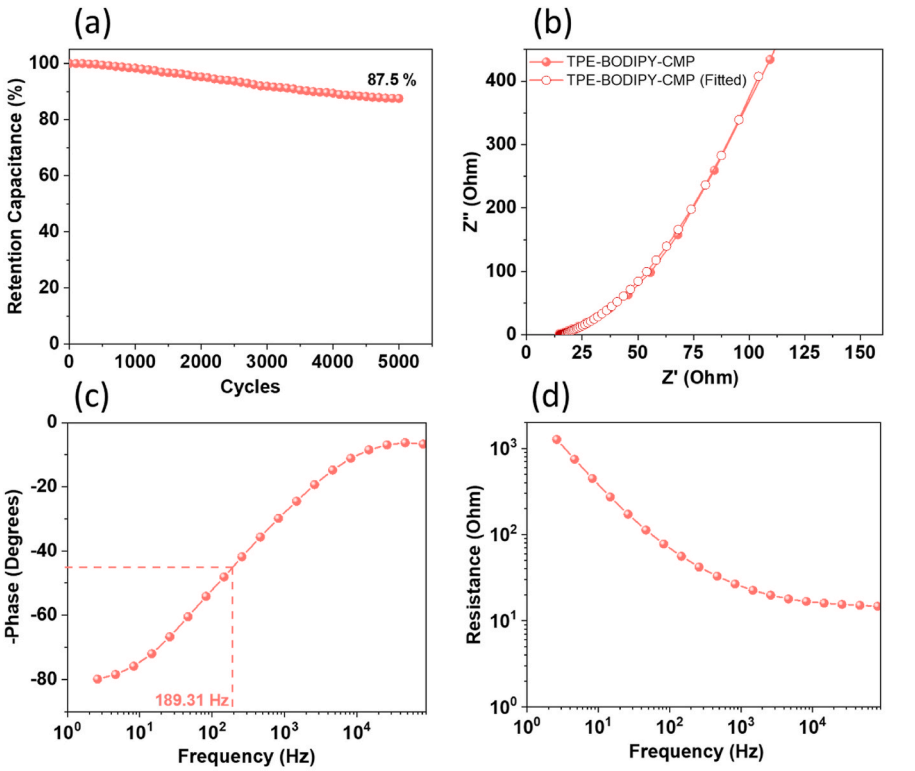

Fig. 5. (a) Retention capacitance, (b) Nyquist plots, (c) Bode plot of frequency-dependent resistance (magnitude), and (d) Bode plot of frequency-dependent phase angles of TPE-BODIPY-CMP.

constructed supercapacitor with different scan rates (5–100 mV s^{-1}) in 1 M aqueous KOH to investigate the electrochemical behavior of TPE-BODIPY-CMP [Fig. 4(a)]. The TPE-BODIPY-CMP exhibited a quasi-rectangular voltammogram form with redox peaks (Fig. 4(a)), indicating a combination of electric double-layer capacitance and pseudo-capacitance properties [80–82]. Notably, TPE-BODIPY-CMP displayed a distinctive humped shape resembling a rectangle, maintaining consistency across the scan rate range. This suggests the stability of TPE-BODIPY-CMP during current sweeps, demonstrating capacitance from EDLCs. The 2D network, abundant heteroatoms, and short diffusion routes within TPE-BODIPY-CMP electrodes facilitated fast charge percolation, ensuring stable and reversible CV even at high scan rates. Galvanostatic charge/discharge (GCD) profiles of TPE-BODIPY-CMP at various current density ranges (0.5–20 A g^{-1}) revealed triangular forms, indicating the predominant energy storage mechanism as EDLC and pseudo-capacitance [Fig. 4(b)]. TPE-BODIPY-CMP exhibited longer discharge times for all currents, demonstrating its superior specific capacitance value (176 F g^{-1}) at 0.5 A g^{-1} [Fig. 4(c)]. The comparison of TPE-BODIPY-CMP's capacity value with various published information concerning three electrode supercapacitor materials is shown in Table S1. Based on the calculation, the TPE-BODIPY-CMP supercapacitor's energy density was determined to be 24.39 Wh kg^{-1}, as shown in Fig. 4(d). The durability during cycling at 10 A g^{-1} for 5000 cycles showcased excellent cycling stability, with a capacitance retention rate of 83.23% for TPE-BODIPY-CMP [Fig. 5(a)]. To assess electric resistance, electrochemical impedance spectroscopy was employed, presenting a Nyquist plot with fitted circuits in Fig. 5(b). The TPE-BODIPY-CMP electrode exhibited an initial ohmic resistance of 14.65 Hz. The Bode plot illustrated the capacitive characteristics of TPE-BODIPY-CMP, with slant lines at low frequency indicating a negative slope and modest resistances at high frequency [Fig. 5(c)]. Furthermore, the frequency-dependent phase angle graphs of various electrodes were presented in Fig. 5(d), with knee frequencies calculated at a phase angle of −45°. The TPE-BODIPY-CMP electrode displayed a knee frequency of 189.31 Hz [Fig. 5(c)], suggesting improved rate performance. Above the knee frequency, the supercapacitor exhibited elevated resistance, aligning with the diffusion of electrolyte ions through the porous network structure of TPE-BODIPY-CMP [83].

3.3. Sensory behavior of TPE-BODIPY-CMP towards metal ions

The emission characteristics of the TPE-BODIPY-CMP exhibit excitation-independent emission patterns across a broad wavelength spectrum ranging from EX 440 to EX 570 [Fig. S17(a)]. This emission behavior is typical in fluorophores or nanomaterials with core-shell structures [84]. Similarly, in larger CMP, the intricate network and incorporation of doped heteroatoms contribute significantly to these fluorescence properties. Furthermore, analysis using the chromaticity color chart [Fig. S17(b)] indicates that the fluorescence colors are predominantly distributed within the near-IR 1 range. The sensory response of TPE-BODIPY-CMP was investigated concerning various cations, including Cu^{2+}, Pb^{2+}, Al^{3+}, Cr^{3+}, Ni^{2+}, Ce^{3+}, Mg^{2+}, Hg^{2+}, Fe^{3+}, Fe^{2+}, Zn^{2+}, and Ag^{+}, in aqueous solutions at neutral pH (7.2). Upon excitation at 480 nm, the polymer exhibited fluorescence emission centered at 592 nm, originating from the BODIPY units. Notably, among the examined cations, only Cu^{2+} demonstrated a quenching effect on the emission of TPE-BODIPY-CMP (quenching efficiency, QE = 53%), as illustrated in Fig. 6(a) and (b). The observed quenching by Cu^{2+} was attributed to its paramagnetism, leading to an energy transfer from coordinated BODIPY units [85]. Fig. 6(c) provides compelling evidence of the distinctive quenching of the hue of TPE-BODIPY-CMP in the presence of Cu^{2+} cations under UV light, contrasting with the behavior observed with other cations.

An evaluation was carried out to examine the influence of Cu^{2+} ions on the fluorescence of TPE-BODIPY-CMP under ideal experimental conditions. To detect the presence of Cu^{2+} ions, a series of

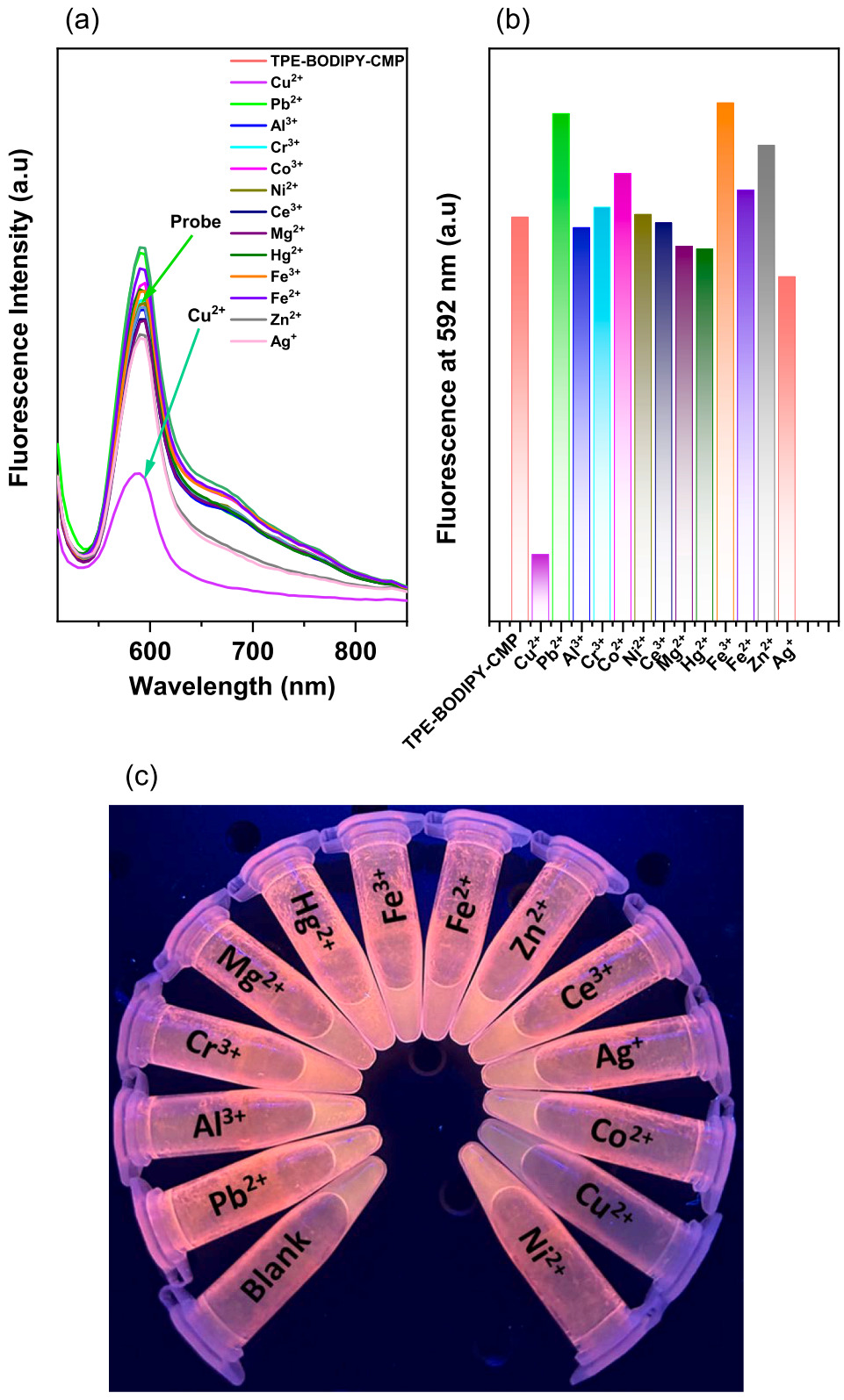

Fig. 6. Effect of cations (aqueous) on (a) the emission spectrum, (b) the emission at 592 nm of the TPE-BODIPY-CMP (water: THF (1:1), HEPES buffer (10^{-3} M), and (c) the color of TPE-BODIPY-CMP with cations under UV lamp ($\lambda_{ex.}$ = 480 nm). (For interpretation of the references to color in this figure legend, the reader is referred to the Web version of this article.)

concentrations ranging from 1 μM to 500 μM were prepared, and the fluorescence intensity of TPE-BODIPY-CMP was measured at 530 nm [see Fig. S18]. Fig. S18 demonstrates the decrease in fluorescence intensity of TPE-BODIPY-CMP with the increasing concentration of Cu^{2+} ions. Furthermore, the sensitivity of TPE-BODIPY-CMP in detecting Cu^{2+} was assessed by plotting the titration of emission at 592 nm against the concentration of Cu^{2+}, as depicted in Fig. 7. LOD = 3σ/b, where b is the slope of the titration plot and σ is the standard deviation of several

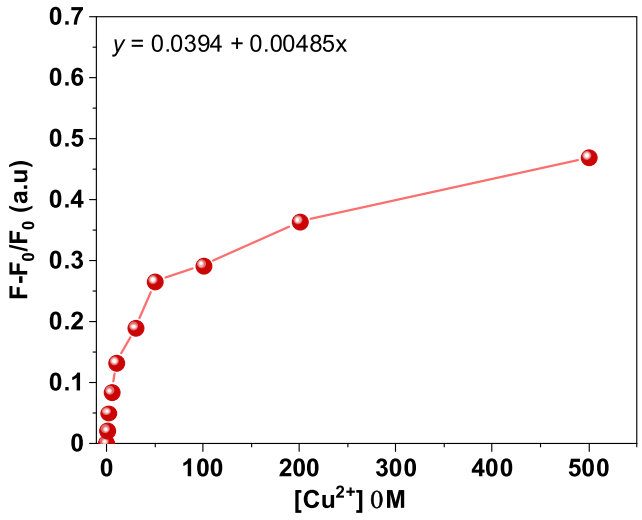

Fig. 7. Effect of Cu^{2+} concentration on the emission at 592 nm of the TPE-BODIPY-CMP (water: THF (1:1), HEPES buffer (10^{-3} M). $\lambda_{ex.} = 480$ nm.

measurements of the TPE-BODIPY-CMP'S emission at 592 nm, was used to calculate LOD. The computed LOD was 2.5×10^{-7} M.

4. Conclusions

In this investigation, the Sonogashira coupling method was employed for the synthesis of a novel TPE-BODIPY-CMP incorporating TPE and BODIPY moieties. The chemical structure of the TPE-BODIPY-CMP framework was verified using FTIR, ssNMR, and XPS techniques. Through BET analysis, it was determined that the TPE-BODIPY-CMP possesses pore diameters ranging from 1.52 to 2.82 nm, a S_{BET} of 300 m^2 $g^{-1,}$ and a uniform granular morphology of the aggregation. The outstanding porosity and fluorescence exhibited by TPE-BODIPY-CMP make it suitable for applications in both electrochemical and sensory fields. Strikingly, TPE-BODIPY-CMP revealed an exceptional capacitance retention, retaining 83.23% of their capacitance even after 5000 cycles. Moreover, among all the cations under the study, only Cu^{2+} quenched the fluorescence emission of TPE-BODIPY-CMP achieving a LOD of 2.5×10^{-7} M.

CRediT authorship contribution statement

Awad I. Said: Formal analysis, Conceptualization. **Mohamed Gamal Mohamed:** Writing – review & editing, Writing – original draft, Supervision, Methodology, Investigation, Formal analysis, Data curation, Conceptualization. **Manivannan Madhu:** Formal analysis, Conceptualization. **Poonam Nagendr Singh:** Investigation. **Swetha V Chaganti:** Investigation. **Mohamed Hammad Elsayed:** Data curation. **Wei Lung Tseng:** Supervision. **Françisco M. Raymo:** Supervision. **Shiao-Wei Kuo:** Supervision.

Declaration of competing interest

The authors declare that they have no known competing financial interests or personal relationships that could have appeared to influence the work reported in this paper.

Data availability

The data that has been used is confidential.

Acknowledgments

This study was supported financially by the National Science and Technology Council, under contracts NSTC 110-2124-M-002-013 and 112-2223-E-110-002. A. I. Said and F. M. Raymo gratefully acknowledge for the financial support of U.S.- Egypt Joint Board (Project ID J167). The authors thank the staff at National Sun Yat-sen University for their assistance with the TEM (ID: EM022600) experiments.

Appendix A. Supplementary data

Supplementary data to this article can be found online at https://doi.org/10.1016/j.polymer.2024.126988.

References

[1] J. Luo, W. Zhong, Y. Zou, C. Xiong, W. Yang, Preparation of morphology-controllable polyaniline and polyaniline/graphene hydrogels for high performance binder-free supercapacitor electrodes, J. Power Sources 319 (2016) 73–81, https://doi.org/10.1016/j.jpowsour.2016.04.004.

[2] M.G. Mohamed, A.M. Elewa, M.S. Li, S.W. Kuo, Construction and multifunctional of hypercrosslinked porous organic polymers containing ferrocene unit for high-performance iodine adsorption and supercapacitor, J. Taiwan Inst. Chem. Eng. 150 (2023) 105045, https://doi.org/10.1016/j.jtice.2023.105045.

[3] A.O. Mousa, M.G. Mohamed, C.H. Chuang, S.W. Kuo, Carbonized Aminal-linked porous organic polymers containing pyrene and triazine units for gas uptake and energy storage, Polymers 15 (2023) 1891, https://doi.org/10.3390/polym15081891.

[4] M.M. Samy, M.G. Mohamed, S.U. Sharma, S.V. Chaganti, T.H. Mansoure, J.T. Lee, T. Chen, S.W. Kuo, Constructing conjugated microporous polymers containing triphenylamine moieties for high-performance capacitive energy storage, Polymer 264 (2023) 125541, https://doi.org/10.1016/j.polymer.2022.125541.

[5] M.G. Mohamed, W.C. Chang, S.V. Chaganti, S.U. Sharma, J.T. Lee, S.W. Kuo, Dispersion of ultrastable crown-ether-functionalized triphenylamine and pyrene-linked porous organic conjugated polymers with single-walled carbon nanotubes as high-performance electrodes for supercapacitors, Polym. Chem. 14 (2023) 4589–4601, https://doi.org/10.1039/D3PY00708A.

[6] M.M. Samy, M.G. Mohamed, S.-W. Kuo, Conjugated microporous polymers based on ferrocene units as highly efficient electrodes for energy storage, Polymers 15 (2023) 1095, https://doi.org/10.3390/polym15051095.

[7] A.O. Mousa, C.-H. Chuang, S.-W. Kuo, M.G. Mohamed, Strategic design and synthesis of ferrocene linked porous organic frameworks toward tunable CO_2 capture and energy storage, Int. J. Mol. Sci. 24 (2023) 12371, https://doi.org/10.3390/ijms241512371.

[8] M.G. Mohamed, S.-Y. Chang, M. Ejaz, M.M. Samy, A.O. Mousa, S.W. Kuo, Design and synthesis of bisulfone-linked two-dimensional conjugated microporous polymers for CO_2 adsorption and energy storage, Molecules 28 (2023) 3234, https://doi.org/10.3390/molecules28073234.

[9] M. Ejaz, M.G. Mohamed, W.C. Huang, S.W. Kuo, Pyrene-based covalent organic polymers with nano carbonaceous composites for efficient supercapacitive energy storage, J. Mater. Chem. A 11 (2023) 22868–22883, https://doi.org/10.1039/D3TA02741D.

[10] C.Y. Chen, M.G. Mohamed, W.C. Chen, S.W. Kuo, Construction of Ultrastable porous carbons materials derived from organic/inorganic double-decker silsesquioxane (DDSQ) hybrid as a high-performance electrode for supercapacitor, Mater. Today Chem. 34 (2023) 101773, https://doi.org/10.1016/j.mtchem.2023.101773.

[11] M. Ejaz, M.G. Mohamed, Y.T. Chen, K. Zhang, S.W. Kuo, Porous carbon materials augmented with heteroatoms derived from hyperbranched biobased benzoxazine resins for enhanced CO_2 adsorption and exceptional supercapacitor performance, J. Energy Storage 78 (2024) 110166, https://doi.org/10.1016/j.est.2023.110166.

[12] M.G. Mohamed, M.M. Samy, T.H. Mansoure, S.U. Sharma, M.S. Tsai, J.H. Chen, J. T. Lee, S.W. Kuo, Dispersions of 1,3,4-oxadiazole-linked conjugated microporous polymers with carbon nanotubes as a high-performance electrode for supercapacitors, ACS Appl. Energy Mater. 5 (2022) 3677–3688, https://doi.org/10.1021/acsaem.2c00100.

[13] P.N. Singh, M.G. Mohamed, S.V. Chaganti, S.U. Sharma, M. Ejaz, J.T. Lee, S. W. Kuo, Rational design of ultrastable conjugated microporous polymers based on pyrene and perylene units as high-performance organic electrode materials for supercapacitor applications, ACS Appl. Energy Mater. 6 (2023) 8277–8287, https://doi.org/10.1021/acsaem.3c01391.

[14] M.G. Mohamed, T.H. Mansoure, M.M. Samy, Y. Takashi, A.A. Mohammed, T. Ahamad, S.M. Alshehri, J. Kim, B.M. Matsagar, K.C.W. Wu, Ultrastable conjugated microporous polymers containing benzobisthiadiazole and pyrene building blocks for energy storage applications, Molecules 27 (2022) 2025, https://doi.org/10.3390/molecules27062025.

[15] T.H. Weng, M.G. Mohamed, S.U. Sharma, S.V. Chaganti, M.M. Samy, J.T. Lee, S. W. Kuo, Ultrastable three-dimensional triptycene-and tetraphenylethene-conjugated microporous polymers for energy storage, ACS Appl. Energy Mater. 5 (2022) 14239–14249, https://doi.org/10.1021/acsaem.2c02809.

[16] M.G. Mohamed, H.Y. Hu, M. Madhu, M.M. Samy, I.M. Mekhemer, W.L. Tseng, H. H. Chou, S.W. Kuo, Ultrastable two-dimensional fluorescent conjugated microporous polymers containing pyrene and fluorene units for metal ion sensing and energy storage, Eur. Polym. J. 189 (2023) 111980, https://doi.org/10.1016/j.eurpolymj.2023.111980.
[17] M. Ejaz, M.G. Mohamed, S.U. Sharma, J.T. Lee, C.F. Huang, T. Chen, S.W. Kuo, An ultrastable porous polyhedral oligomeric silsesquioxane/tetraphenylthiophene hybrid as a high-performance electrode for supercapacitors, Molecules 27 (2022) 6238, https://doi.org/10.3390/molecules27196238.
[18] A.O. Mousa, Z.I. Lin, S.V. Chaganti, C.H. Chuang, C.K. Chen, S.W. Kuo, M. G. Mohamed, Bifunctional imidazolium linked tetraphenylethene based conjugated microporous polymers for dynamic antibacterial properties and supercapacitor electrode, Polym. Chem. 15 (2024) 397–411, https://doi.org/10.1039/D3PY01303K.
[19] X. Cai, Q. Ren, W. Sun, F. Yang, High-performance activated carbons for supercapacitor: effects of porous structures, heteroatom doping, and morphology, Int. J. Energy Res. 45 (2021) 21414–21434, https://doi.org/10.1002/er.7191.
[20] G.P. Hao, F. Hippauf, M. Oschatz, F.M. Wisser, A. Leifert, W. Nickel, N.M. Noriega, Z. Zheng, S. Kaskel, Stretchable and semitransparent conductive hybrid hydrogels for flexible supercapacitors, ACS Nano 8 (2014) 7138–7146, https://doi.org/10.1021/nn502065u.
[21] Y.B. He, G.R. Li, Z.L. Wang, C.Y. Su, Y.X. Tong, Single-crystal ZnO nanorod/amorphous and nanoporous metal oxide shell composites: controllable electrochemical synthesis and enhanced supercapacitor performances, Energy Environ. Sci. 4 (2011) 1288–1292, https://doi.org/10.1039/C0EE00669F.
[22] M.M. Samy, M.G. Mohamed, S.W. Kuo, Directly synthesized nitrogen-and-oxygen–doped microporous carbons derived from a bio-derived polybenzoxazine exhibiting high-performance supercapacitance and CO_2 uptake, Eur. Polym. J. 138 (2020) 109954, https://doi.org/10.1016/j.eurpolymj.2020.109954.
[23] B. Zhu, B. Liu, C. Qu, H. Zhang, W. Guo, Z. Liang, F. Chen, R. Zou, Tailoring biomass-derived carbon for high-performance supercapacitors from controllably cultivated algae microspheres, J. Mater. Chem. A 6 (2018) 1523–1530, https://doi.org/10.1039/C7TA09608A.
[24] Y. Deng, Y. Xie, K. Zou, X. Ji, Review on recent advances in nitrogen-doped carbons: preparations and applications in supercapacitors, J. Mater. Chem. A 4 (2016) 1144–1173, https://doi.org/10.1039/C5TA08620E.
[25] C. Zhang, Y. Yongwu, P. Mu, X. Wang, Q. He, Y. Chen, J. Zeng, F. Wang, Y. Xu, J. X. Jiang, Toward high performance thiophene-containing conjugated microporous polymer anodes for lithium-ion batteries through structure design, Adv. Funct. Mater. 28 (2018) 1705432, https://doi.org/10.1002/adfm.201705432.
[26] D.W. Wang, F. Feng, Z.G. Chen, G.Q. Lu, H.M. Cheng, Synthesis and electrochemical property of boron-doped mesoporous carbon in supercapacitor, Chem. Mater. 20 (2008) 7195–7200, https://doi.org/10.1021/cm801729y.
[27] P.R. Deshmukh, N.M. Shinde, S.V. Patil, R.N. Bulakhe, C.D. Lokhande, Supercapacitive behavior of polyaniline thin films deposited on fluorine doped tin oxide (FTO) substrates by microwave-assisted chemical route, Chem. Eng. J. 223 (2013) 572–577, https://doi.org/10.1016/j.cej.2013.03.056.
[28] M.R. Benzigar, S.N. Talapaneni, S. Joseph, K. Ramadass, G. Singh, J. Scaranto, U. Ravon, K. Al-Bahily, A. Vinu, Recent advances in functionalized micro and mesoporous carbon materials: synthesis and applications, Chem. Soc. Rev. 47 (2018) 2680–2721, https://doi.org/10.1039/C7CS00787F.
[29] D.H. Jurcakova, D.M. Kodama, S. Shiraishi, H. Hatori, Z.H. Zhu, G.Q. Lu, Nitrogen-enriched nonporous carbon electrodes with extraordinary supercapacitance, Adv. Funct. Mater. 19 (2009) 1800–1809, https://doi.org/10.1002/adfm.200801100.
[30] W. Na, J. Jaemoon, J.W. Park, G.P. Lee, J. Jang, Highly porous carbon nanofibers co-doped with fluorine and nitrogen for outstanding supercapacitor performance, J. Mater. Chem. A 5 (2017) 17379–17387, https://doi.org/10.1039/C7TA04406B.
[31] H. Jurcakova, M.S. Denisa, G.Q. Lu, N.K.A.C. Kodiweera, P.E. Stallworth, S. Greenbaum, T.J. Bandosz, Effect of surface phosphorus functionalities of activated carbons containing oxygen and nitrogen on electrochemical capacitance, Carbon 47 (2009) 1576–1584, https://doi.org/10.1016/j.carbon.2009.02.006.
[32] M.G. Mohamed, M.H. Elsayed, Y. Ye, M.M. Samy, A.E. Hassan, T.H. Mansoure, Z. Wen, H.H. Chou, K.H. Chen, S.W. Kuo, Construction of porous organic/inorganic hybrid polymers based on polyhedral oligomeric silsesquioxane for energy storage and hydrogen production from water, Polymers 15 (2022) 182, https://doi.org/10.3390/polym15010182.
[33] W.T. Chung, I.M.A. Mekhemer, M.G. Mohamed, A.M. Elewa, A.F.M. EL-Mahdy, H. H. Chou, S.W. Kuo, K.C.W. Wu, Recent advances in metal/covalent organic frameworks based materials: their synthesis, structure design and potential applications for hydrogen production, Coord. Chem. Rev. 483 (2023) 215066, https://doi.org/10.1016/j.ccr.2023.215066.
[34] A.O. Mousa, M.G. Mohamed, Z.I. Lin, C.H. Chuang, C.K. Chen, S.W. Kuo, Construction of cationic conjugated microporous polymers containing pyrene units through post-cationic modification for enhanced antibacterial performance, J. Taiwan Inst. Chem. Eng. 157 (2024) 105448, https://doi.org/10.1016/j.jtice.2024.105448.
[35] M.G. Mohamed, M.H. Elsayed, C.J. Li, A.E. Hassan, I.M.A. Mekhemer, A.F. Musa, M.K. Hussien, L.C. Chen, K.H. Chen, H.H. Chou, S.W. Kuo, Reticular design and alkyne bridge engineering in donor–π–acceptor type conjugated microporous polymers for boosting photocatalytic hydrogen evolution, J. Mater. Chem. A (2024), https://doi.org/10.1039/D3TA07309B.
[36] M.M. Samy, I.M.A. Mekhemer, M.G. Mohamed, M.H. Elsayed, K.H. Lin, Y.K. Chen, T.L. Wu, H.H. Chou, S.W. Kuo, Conjugated microporous polymers incorporating Thiazolo[5,4-d]thiazole moieties for Sunlight-Driven hydrogen production from water, Chem. Eng. J. 446 (2022) 137158, https://doi.org/10.1016/j.cej.2022.137158.
[37] C.W. Hsiao, A.M. Elewa, M.G. Mohamed, S.W. Kuo, Highly stable hybrid porous polymers containing polyhedral oligomeric silsesquioxane (POSS)/Dibenzo [g, p] chrysene and Dibenzo [b, d] thiophene units for efficient Rhodamine B dye removal, Sep. Purif. Technol. 332 (2024) 125771, https://doi.org/10.1016/j.seppur.2023.125771.
[38] S.Y. Chang, A.M. Elewa, M.G. Mohamed, I.M.A. Mekhemer, M.M. Samy, K. Zhang, H.H. Chou, S.W. Kuo, Rational design and synthesis of bifunctional Dibenzo[g,p] chrysene-based conjugated microporous polymers for energy storage and visible light-driven photocatalytic hydrogen evolution, Mater. Today Chem. (33) (2023) 101680, https://doi.org/10.1016/j.mtchem.2023.101680.
[39] M.G. Mohamed, M.M. Samy, T.H. Mansoure, C.J. Li, W.C. Li, J.H. Chen, K. Zhang, S.W. Kuo, Microporous carbon and carbon/metal composite materials derived from bio-benzoxazine-linked precursor for CO_2 capture and energy storage applications, Int. J. Mol. Sci. 23 (2022) 347, https://doi.org/10.3390/ijms23010347.
[40] M.G. Mohamed, S.U. Sharma, C.H. Yang, M.M. Samy, A.A.K. Mohammed, S. V. Chaganti, J.T. Lee, S.W. Kuo, Anthraquinone-Enriched conjugated microporous polymers as organic cathode materials for high-performance lithium-ion batteries, ACS Appl. Energy Mater. 4 (2021) 14628–14639, https://doi.org/10.1021/acsaem.1c03270.
[41] M.G. Mohamed, S.V. Chaganti, M.S. Li, M.M. Samy, S.U. Sharma, J.T. Lee, M. H. Elsayed, H.H. Chou, S.W. Kuo, Ultrastable porous organic polymers containing thianthrene and pyrene units as organic electrode materials for supercapacitors, ACS Appl. Energy Mater. 5 (2022) 6442–6452, https://doi.org/10.1021/acsaem.2c00942.
[42] S.U. Sharma, M.H. Elsayed, I.M.A. Mekhemer, T.S. Meng, H.H. Chou, S.W. Kuo, M. G. Mohamed, Rational design of pyrene and thienyltriazine-based conjugated microporous polymers for high-performance energy storage and visible-light photocatalytic hydrogen evolution from water, Giant 17 (2024) 100217, https://doi.org/10.1016/j.giant.2023.100217.
[43] M.G. Mohamed, C.C. Chen, K. Zhang, S.W. Kuo, Construction of three-dimensional porous organic polymers with enhanced CO_2 uptake performance via solid-state thermal conversion from tetrahedral benzoxazine-linked precursor, Eur. Polym. J. 200 (2023) 112551, https://doi.org/10.1016/j.eurpolymj.2023.112551.
[44] P.N. Singh, M.G. Mohamed, S.W. Kuo, Systematic design and synthesis of conjugated microporous polymers containing pyrene and azobenzene building materials for high-performance energy storage, ACS Appl. Energy Mater. 6 (2023) 11342–11351, https://doi.org/10.1021/acsaem.3c02252.
[45] M.G. Mohamed, E.C.A. Jr, B.M. Matsagar, J. Na, Y. Yamauchi, K.C.W. Wu, S. W. Kuo, Construction hierarchically mesoporous/microporous materials based on block copolymer and covalent organic framework, J. Taiwan Inst. Chem. Eng. 112 (2020) 180–192, https://doi.org/10.1016/j.jtice.2020.06.013.
[46] A. Treibs, F.H. Kreuzer, Difluorboryl-Komplexe von Di- und Tripyrrylmethenen, Justus Liebigs Ann. Chem. 718 (1968) 208, https://doi.org/10.1002/jlac.19687180119.
[47] A. Loudet, K. Burgess, BODIPY dyes and their derivatives: syntheses and spectroscopic properties, Chem. Rev. 107 (2007) 4891–4932, https://doi.org/10.1021/cr078381n.
[48] M. Poddar, R. Misra, Recent advances of BODIPY based derivatives for optoelectronic applications, Coord. Chem. Rev. 421 (2020) 213462, https://doi.org/10.1016/j.ccr.2020.213462.
[49] Y. Ni, J. Wu, Far-red and near infrared BODIPY dyes: synthesis and applications for fluorescent pH probes and bio-imaging, Org. Biomol. Chem. 12 (2014) 3774–3791, https://doi.org/10.1039/C3OB42554A.
[50] Sarasija Das, S. Dey, S. Patra, A. Bera, T. Ghosh, B. Prasad, K.D. Sayala, K. Maji, A. Bedi, S. Debnath, BODIPY-based molecules for biomedical applications, Biomolecules 13 (2023) 1723, https://doi.org/10.3390/biom13121723.
[51] R.W. Wagner, J.S. Lindsey, Boron-dipyrromethene dyes for incorporation in synthetic multi-pigment light-harvesting arrays, Pure Appl. Chem. 68 (1996) 1373–1380, https://doi.org/10.1351/pac199668071373.
[52] G. Beer, K. Rurack, J. Daub, Chiral discrimination with a fluorescent boron–dipyrromethene, Chem. Commun. (2001) 1138–1139, https://doi.org/10.1039/B102376B.
[53] J. Wang, Q. Gong, L. Jiao, E. Hao, Research advances in BODIPY-assembled supramolecular photosensitizers for photodynamic therapy, Coord. Chem. Rev. 496 (2023) 215367, https://doi.org/10.1016/j.ccr.2023.215367.
[54] T.A. Golovkova, D.V. Kozlov, D. C Neckers, Synthesis and properties of novel fluorescent switches, J. Org. Chem. 70 (2005) 5545, https://doi.org/10.1021/jo050540k.
[55] R.Y. Lai, A.J. Bard, Electrogenerated chemiluminescence 71. Photophysical, electrochemical, and electrogenerated chemiluminescent properties of selected Dipyrromethene−BF_2 dyes, J. Phys. Chem. B 107 (2003) 5036–5042, https://doi.org/10.1021/jp034578h.
[56] T. Chen, J.H. Boyer, M.L. Trudell, Synthesis of 2,6-diethyl-3-methacroyloxymethyl-1,5,7,8-tetramethylpyrromethene-BF_2 for the preparation of new solid-state laser dyes, Heteroat. Chem. 8 (1997) 51, https://doi.org/10.1002/(SICI)1098-1071(1997)8:1<51::AID-HC7>3.0.CO;2-5.
[57] A. Amboise, C. Kirmaier, R.W. Wagner, R.S. Loewe, D.F. Bocian, D. Holten, J. S. Lindsey, Weakly coupled molecular photonic wires: synthesis and excited-state energy-transfer dynamics, J. Org. Chem. 67 (2002) 3811, https://doi.org/10.1021/jo025561i.
[58] S. Hattori, K. Ohkubo, Y. Urano, H. Sunahara, T. Nagano, Y. Wada, N.V. Tkchanko, H. Lemmetyinen, S. Fukuzumi, Charge separation in a nonfluorescent Donor−Acceptor dyad derived from boron dipyrromethene dye, leading to photocurrent generation, J. Phys. Chem. B 109 (2005) 15368–15375, https://doi.org/10.1021/jp050952x.

[59] N. Boens, V. Volker Leen, W. Dehaen, Fluorescent indicators based on BODIPY, Chem. Soc. Rev. 413 (2012) 1130–1172, https://doi.org/10.1039/C1CS15132K.
[60] D.G. Wang, H. Wang, M. Song, G. Yu, G.C. Kuang, BODIPY-based carbonaceous materials for high performance electrical capacitive energy storage, Chem. Asian J. 13 (2018) 3051–3056, https://doi.org/10.1002/asia.201801094.
[61] M.G. Mohamed, H.Y. Hu, S. Santhoshkumar, M. Madhu, T.H. Mansoure, C. W. Hsiao, Y. Ye, C.W. Huang, W.L. Tseng, S.W. Kuo, Design and synthesis of bifunctional conjugated microporous polymers containing tetraphenylethene and bisulfone units for energy storage and fluorescent sensing of *p*-nitrophenol, Colloids Surf. A Physicochem. Eng. Asp. 680 (2024) 132675, https://doi.org/10.1016/j.colsurfa.2023.132675.
[62] P. Wang, X. Miao, Y. Meng, Q. Wang, J. Wang, H. Duan, Y. Li, C. Li, J. Liu, L. Cao, Tetraphenylethene-based supramolecular coordination frameworks with aggregation-induced emission for an artificial light-harvesting system, ACS Appl. Mater. Interfaces 12 (2020) 22630–22639, https://doi.org/10.1021/acsami.0c04917.
[63] M. Selvaraj, K. Rajalakshmi, D.H. Ahn, S.J. Yoon, Y.S. Nam, Y. Lee, Y. Xu, J. W. Song, K.B. Lee, Tetraphenylethene-based fluorescent probe with aggregation-induced emission behavior for Hg^{2+} detection and its application, Anal. Chim. Acta 1148 (2021) 238178, https://doi.org/10.1016/j.aca.2020.12.053.
[64] J. Bai, J. Peng, T. Xu, M. Bu, W. Chen, Y. Nie, J. Jia, A tetraphenylethene-based Schiff base AIEgen with a large Stokes shift as probe for highly sensitive and selective detection of aqueous Cu^{2+} ions and its application in cell imaging, Spectrochim. Acta Mol. Biomol. Spectrosc. 290 (2023) 122190, https://doi.org/10.1016/j.saa.2022.122190.
[65] D. Pan, Y. Don, Y. Lu, G. Xiao, H. Chi, Z. Hu, AIE fluorescent probe based on tetraphenylethylene and morpholine-thiourea structures for detection of HClO, Anal. Chim. Acta 1235 (2022) 340559, https://doi.org/10.1016/j.aca.2022.340559.
[66] Y. Xiao, K. Zheng, N. Zhang, Y. Wang, J. Yan, D. Wang, X. Liu, Facile synthesis of tetraphenylethene (TPE)-Based fluorophores derived by π-extended systems: opposite mechanofluorochromism, anti-counterfeiting and bioimaging, Eur. J. Chem. 29 (2023) e202203772, https://doi.org/10.1002/chem.202203772.
[67] S. Feng, Q. Gao, X. Gao, J. Yin, Y. Jiao, Fluorescent sensor for copper(II) ion based on coumarin derivative and its application in cell imaging, Inorg. Chem. Commun. 102 (2019) 51–56, https://doi.org/10.1016/j.inoche.2019.01.012.
[68] S. Lutsenko, Atp7b-/- mice as a model for studies of Wilson's disease, Biochem. Soc. Trans. 36 (2008) 1233–1238, https://doi.org/10.1042/BST0361233.
[69] M. Savelieff, S. Lee, Y. Liu, M. Lim, Untangling amyloid-β, tau, and metals in Alzheimer's disease, ACS Chem. Biol. 8 (2013) 856–865, https://doi.org/10.1021/cb400080f.
[70] A.I. Said, N. Georgiev, V.B. Bojinov, Low molecular weight probe for selective sensing of PH and Cu^{2+} working as three INHIBIT based digital comparator, J. Fluoresc. 32 (2022) 405–417, https://doi.org/10.1007/s10895-021-02856-4.
[71] A.I. Said, N. Georgiev, V.B. Bojinov, Sensor activity and logic behavior of dihydroxyphenylhydrazone derivative as a chemosensor for Cu^{2+} determination in alkaline aqueous solutions, J. Photochem. Photobiol., A: Chem 311 (2015) 16–24, https://doi.org/10.1016/j.jphotochem.2015.05.035.
[72] A.I. Said, N. Georgiev, V.B. Bojinov, Synthesis of a single 1,8-naphthalimide fluorophore as a molecular logic lab for simultaneously detecting of Fe^{3+}, Hg^{2+} and Cu^{2+}, Spectrochim. Acta Mol. Biomol. Spectrosc. 196 (2018) 76–82, https://doi.org/10.1016/j.saa.2018.02.005.
[73] A.I. Said, N. Georgiev, V.B. Bojinov, A smart chemosensor: discriminative multidetection and various logic operations in aqueous solution at biological PH, Spectrochim. Acta Mol. Biomol. Spectrosc. 223 (2019) 117304–117313, https://doi.org/10.1016/j.saa.2019.117304.
[74] N. Georgiev, N, A.I. Said, R. Toshkova, R. Tzoneva, V.B. Bojinov, A novel water-soluble perylenetetracarboxylic diimide as a fluorescent pH probe: chemosensing, biocompatibility and cell imaging, Dyes Pigments 160 (2019) 28–36, https://doi.org/10.1016/j.dyepig.2018.07.048.
[75] A.I. Said, N.I. Georgiev, V.B. Bojinov, A novel dual naked eye colorimetric and fluorescent pH chemosensor and its ability to execute three INHIBIT based digital comparator, Dyes Pigments 205 (2022) 110489, https://doi.org/10.1016/j.dyepig.2022.110489.
[76] A.I. Said, D. Staneva, S. Angelova, I. Grabchev, Self-associated 1,8-naphthalimide as a selective fluorescent chemosensor for detection of high pH in aqueous solutions and their Hg^{2+} contamination, Sensors 23 (2023) 399, https://doi.org/10.3390/s23010399.
[77] M.G. Mohamed, W.C. Chang, S.W. Kuo, Crown ether- and benzoxazine-linked porous organic polymers displaying enhanced metal ion and CO_2 capture through solid-state chemical transformation, Macromolecules 55 (2022) 7879–7892, https://doi.org/10.1021/acs.macromol.2c01216.
[78] M.G. Mohamed, S.V. Chaganti, S.U. Sharma, M.M. Samy, M. Ejaz, J.T. Lee, K. Zhang, S.W. Kuo, Constructing conjugated microporous polymers containing the pyrene-4,5,9,10-tetraone unit for energy storage, ACS Appl. Energy Mater. 5 (2022) 10130–10140, https://doi.org/10.1021/acsaem.2c01842.
[79] M.G. Mohamed, T.C. Chen, S.W. Kuo, Solid-state chemical transformations to enhance gas capture in benzoxazine-linked conjugated microporous polymers, Macromolecules 54 (2021) 5866–5877, https://doi.org/10.1021/acs.macromol.1c00736.
[80] M.M. Samy, Maha M.G. Mohamed, S.W. Kuo, Pyrene-functionalized tetraphenylethylene polybenzoxazine for dispersing single-walled carbon nanotubes and energy storage, Compos. Sci. Technol. 199 (2020) 108360, https://doi.org/10.1016/j.compscitech.2020.108360.
[81] Y. Li, S. Zheng, X. Liu, P. Li, L. Sun, R. Yang, S. Wang, Z.S. Wu, X. Bao, W.Q. Deng, Conductive microporous covalent triazine-based framework for high-performance electrochemical capacitive energy storage, Angew. Chem. Int. Ed. 130 (2018) 8124–8128, https://doi.org/10.1002/anie.201711169.
[82] Y. Liu, X. Hao, L. Wang, Y. Xu, J. Liu, X. Tian, B. Yao, Facile synthesis of porous carbon materials with extra high nitrogen content for supercapacitor electrodes, New J. Chem. 43 (2019) 3713–3718, https://doi.org/10.1039/C8NJ05718D.
[83] R. Xu, F. Guo, X. Cui, L. Zhang, K. Wang, J. Wei, High performance carbon nanotube based fiber-shaped supercapacitors using redox additives of polypyrrole and hydroquinone, J. Mater. Chem. A 3 (2015) 22353–22360, https://doi.org/10.1039/C5TA06165B.
[84] M. Madhu, T.H. Chen, W.L. Tseng, White-light emission of single carbon dots prepared by hydrothermal carbonization of poly(diallyldimethylammonium chloride): applications to fabrication of white-light-emitting films, J. Colloid Interface Sci. 556 (2019) 120–127, https://doi.org/10.1016/j.jcis.2019.08.049.
[85] Y. Xiang, Z. Li, X. Chen, A. Tong, Highly sensitive and selective optical chemosensor for determination of Cu^{2+} in aqueous solution, Talanta 74 (2008) 1148–1153, https://doi.org/10.1016/j.talanta.2007.08.018.